

Electrostatic fluctuation and fluctuation-induced particle flux during formation of the edge transport barrier in the JFT-2M tokamak

T. Ido 1), Y. Miura 2), K. Hoshino 2), Y. Hamada 1), Y. Nagashima 1), H. Ogawa 2), K. Shinohara 2), K. Kamiya 2), A. Nishizawa 1), Y. Kawasumi 1), Y. Kusama 2), JFT-2M group 2)

1) National Institute for Fusion Science, Oroshi-cho, Toki-shi, Gifu, 509-5292, Japan

2) Naka Fusion Research Establishment, Japan Atomic Energy Research Institute, Naka-machi, Naka-gun, Ibaraki 311-0193, Japan

e-mail contact of main author : ido@LHD.nifs.ac.jp

Abstract. The electrostatic fluctuation with Geodesic-Acoustic-Mode (GAM) frequency is observed in L-mode plasmas. The fluctuation has the poloidal wave number (k_θ) of $(-2 \pm 24) \times 10^{-3} \text{ (cm}^{-1}\text{)}$, that corresponds to the poloidal mode number of 1.5 or less, and the radial wave number (k_r) of $0.94 \pm 0.05 \text{ (cm}^{-1}\text{)}$, that is corresponds to $k_r \rho_i = 0.26 < 1$. The amplitude of the fluctuation changes in the radial direction; it is small near the separatrix and it has maximum at 3 cm inside the separatrix. The relation between the amplitude of potential fluctuation and that of density fluctuation is the same as that of the predicted GAM. The fluctuation is probably GAM.

The envelope of ambient density fluctuation and the potential fluctuation have a significant coherence at the GAM frequency. Thus, it is clearly verified that the fluctuation with the GAM frequency correlates with the ambient density fluctuation. The fluctuation with the GAM frequency affects the particle transport through the modulation of the ambient fluctuation. But the effect is not large, and it is not a sufficient condition to form the edge transport barrier and to drive the intermittent particle flux.

1 Introduction

It is thought that the transport of magnetically confined plasmas is mainly caused by plasma turbulence. The clarification of the feature of the turbulence is an important issue to predict the transport of plasma and to estimate the performance of future machines such as International Thermonuclear Experimental Reactor (ITER).

Recently, zonal flow [1] is getting a lot of attention as a cause of the saturation of the turbulence through the energy transfer due to the nonlinear coupling of the turbulence and through the suppression of turbulence due to the shear of zonal flow [2, 3]. Some experimental results indicate the existence of zonal flow [4, 5, 6, 7, 8].

In this study, the potential and density fluctuations are measured directly and simultaneously with a heavy ion beam probe (HIBP), and the existence of Geodesic-Acoustic-Mode (GAM) [9, 10] which is a branch of zonal flow is investigated. Moreover, the correlation between GAM and ambient fluctuation is examined directly, and the influence on the particle flux is studied.

2 Experimental Setup

The HIBP can measure a local electrostatic potential (ϕ) directly even in high temperature plasmas with a high temporal and spatial resolution. Singly charged heavy ion beam, called the primary beam, is injected into the magnetically confined plasma. A part of the primary beam is charged doubly through the electron impact ionization and it is called the secondary beam. Since the charge number increases by one, the total energy of the ion changes by the potential energy at the ionization point. Therefore, ϕ at the ionization point can be obtained through the measurement of the difference in the kinetic energies between the primary and the secondary beam ion. Moreover, the secondary beam current (I_{HIBP}) reflects the electron density

and temperature. In this experiment, the contribution of the temperature is smaller than that of the density [11]. Thus, the density fluctuation \tilde{n}_e can be inferred through the fluctuation of the secondary beam current (\tilde{I}_{HIBP}). When the path integral effect is negligible, the normalized \tilde{I}_{HIBP} is equivalent to the normalized \tilde{n}_e ; $\tilde{n}_e/n_{e,0} \sim \tilde{I}_{HIBP}/I_{HIBP,0}$.

In this study, the characteristics of the electrostatic fluctuation, especially focusing the fluctuation with the GAM frequency, are studied with the HIBP [12] in the JFT-2M tokamak.

The JFT-2M tokamak is a medium-sized tokamak with a major radius (R) of 1.3 m and an averaged minor radius (a) of 0.3 m. The experiments are performed with an upper single null divertor configuration and ∇B drift of ion is toward X-point. The fueling gas species is deuterium.

The HIBP on JFT-2M can measure 7 sample volumes simultaneously: the density fluctuation can be measured in all the 7 sample volumes and the potential can be measured in 4 or 5 sample volumes of them, which depends on the injection condition. The radial width of each sample volume is about 6 mm according to a beam trajectory calculation [13]. The arrangement of sample volumes is determined through the Larmor radius of the beam, that is the combination of the magnetic field strength (B_t) and the beam energy (W_0). When $W_0 = 350$ keV, the sample volumes are aligned in nearly minor-radius-direction in B_t of 1.17 T and in the poloidal direction in B_t of 1.28 T. In addition to that, the sample volumes can be moved in the radial direction with the electrostatic sweeper. Thus, the radial profile in wide range are measured through changing the sweep voltage.

3 Temporal behavior and frequency spectra of the electrostatic fluctuation

First, the temporal behavior of the electrostatic fluctuation is shown. Figure 1 shows the temporal behavior of a typical discharge. In this shot, $B_t = 1.17$ T, the plasma current is 190 kA and the q_{95} , which is the safety factor at the flux surface that encloses 95 % of the total poloidal flux, is 2.9. The neutral beam (NB) is injected in the co-direction from 700 ms to 800 ms and its power is 700 kW.

After the sawtooth crash at 725 ms, large spikes start to appear in D_α intensity and negative spikes are shown in I_{HIBP} . It indicates that the formation of the transport barrier starts intermittently but it is not sustained. The SX intensity from the scrape off layer (SOL) and D_α intensity drop clearly after a sawtooth crash at 735.5 ms. They indicate the transition to the ELM-free H-mode. The fluctuation in the intensity of the secondary beam, which reflects density fluctuation (\tilde{n}_e), exists with the broad frequency spectrum in L-mode, and it is suppressed at the L-H transition (Fig.1(d)). The potential fluctuation($\tilde{\phi}$) shows the similar behavior except that a significant fluctuation with the frequency of about 15 kHz is observed during L-mode (702 - 725 ms) (Fig.1(f)). The potential fluctuation with the frequency of 15 kHz exists in L-mode (and Ohmic phase in other discharge) and disappear at about 725 ms, when the intermittent formation of the transport barrier starts.

4 Characteristics of electrostatic fluctuation with the GAM frequency

4.1 Frequency spectra

The power spectra of the potential ($\tilde{\phi}$) and normalized density fluctuations (\tilde{n}_e/n_{e0}) are shown in Fig.1(g) and (h). A significant peak with the frequency of about 15 kHz appears. The predicted GAM frequency ($\sqrt{(T_i + T_e)}/M_i/2\pi R$) [10] is 19 kHz, where M_i is the mass of the ion, R is 1.54 m, the ion temperature (T_i) is 340 ± 40 eV measured with charge exchange

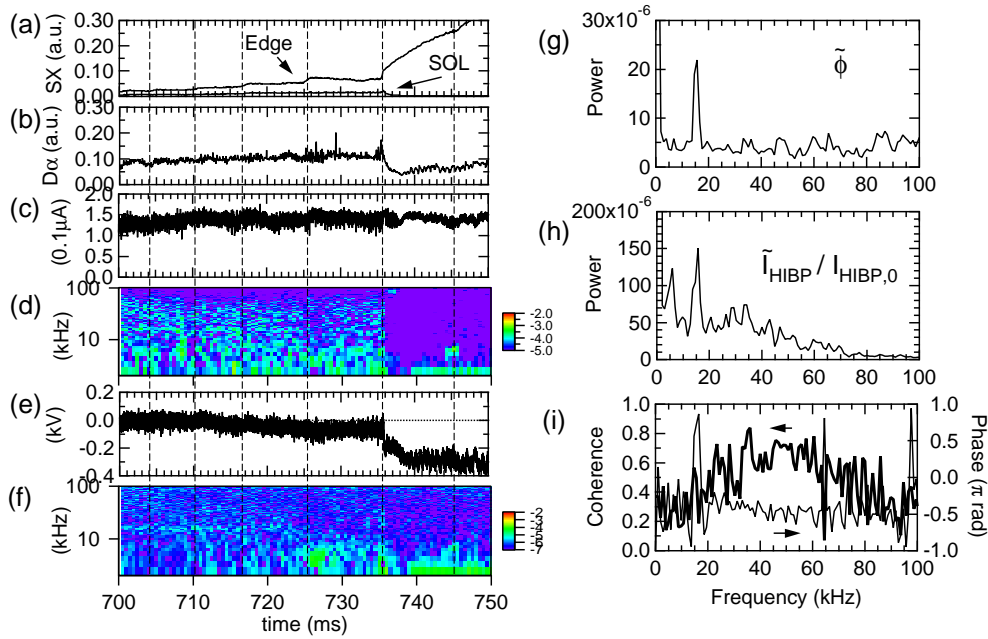


Fig. 1: (a) Chord integrated soft x-ray(SX) intensities from the edge ($\rho \sim 0.85$) and SOL ($\rho \sim 1.1$), where ρ is the distance of the chord from the plasma center normalized by the minor radius. (b) D_{α} intensity in the divertor. The vertical dashed lines indicate the timing of the sawteeth crash. (c)(d) the secondary beam intensity (I_{HIBP}) and its spectrum at 1.4 cm inside the separatrix and its spectrum, (e)(f) electrostatic potential (ϕ). (g)(h) power spectra of the electrostatic potential fluctuation ($\tilde{\phi}$) and fluctuation of normalized I_{HIBP} , which is normalized density fluctuation ($\tilde{n}_e/n_{e,0}$), during L-mode, (i) coherence between $\tilde{\phi}$ and normalized \tilde{I}_{HIBP}

spectroscopy (CXS), and the electron temperature (T_e) is assumed to be the same as T_i . The frequency of the peak in the power spectra is similar to the predicted GAM frequency. The word ‘‘GAM frequency’’ and f_{GAM} are used as the frequency of the peak near the predicted GAM frequency in this paper, and the physical value (A) with the GAM frequency is expressed as $A(f_{GAM})$.

The coherence and phase difference between $\tilde{\phi}$ and $\tilde{n}_e/n_{e,0}$ is shown in Fig.1(c). The fluctuations with the broad frequency spectrum indicate high coherence, and the phase difference is near $\pi/2$. On the other hand, the fluctuations with f_{GAM} indicate lower coherence than the above fluctuation, but the coherence is higher than that of the ambient fluctuation around f_{GAM} . The phase difference is π , and it is quite different from the phase difference of the fluctuations with the broad frequency. The results mean the fluctuations consist of 2 different components at least; one is the fluctuation with the GAM frequency and the other is the ambient fluctuation with the broad frequency spectrum.

4.2 Radial profile of the amplitude

The radial profile of the amplitude of the potential fluctuation with the GAM frequency ($\tilde{\phi}(f_{GAM})$) is measured. The HIBP can measure the potential at 4 sample volumes simultaneously. The sample volumes range over about 1 cm in the radial direction, when they are aligned in nearly radial direction. In order to measure the radial profile of the amplitude of $\tilde{\phi}(f_{GAM})$, the positions of the sample volumes are changed every shot. The profile is shown in Fig.2(b), where each shot is identified with different marks. The amplitude is almost the same in same position

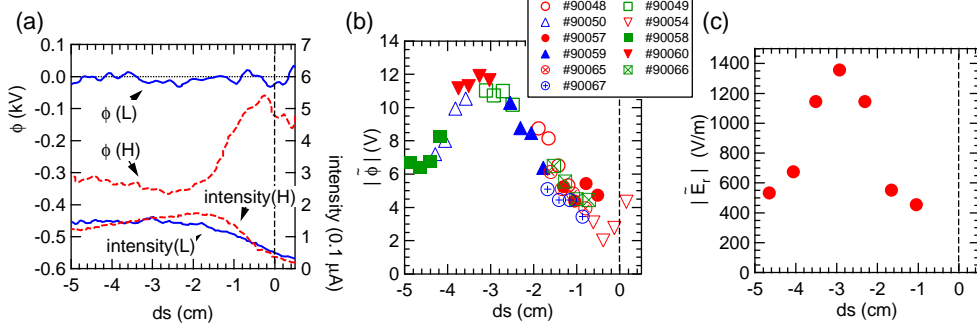


Fig. 2: (a) The radial profiles of ϕ and I_{HIBP} in L- and H-mode. (b) The radial profiles of the amplitude of $\tilde{\phi}(f_{GAM})$ and (c) the radial profile of $\tilde{E}_r(f_{GAM})$ in L-mode. The horizontal axis is the distance from the separatrix and the negative sign means the inside of the separatrix.

even in the different shot, thus the shots are reproducible. The the amplitude of $\tilde{\phi}(f_{GAM})$ is small near the separatrix, it reaches to the maximum value at about 3 cm inside the separatrix.

The radial electric field fluctuation (\tilde{E}_r) can be also measured and the radial profile of its amplitude is shown in Fig.2(c). The profiles is similar to that of $\tilde{\phi}(f_{GAM})$. The maximum of the \tilde{E}_r is about 5 % of the stationary electric field in H-mode plasma [14, 15], and the peak of the profile is inside the position where the steady $E \times B$ flow shear is maximum in H-mode. It indicate the $\tilde{E}_r(f_{GAM})$ may not be very important for L-H transition.

4.3 Coherence in the poloidal direction

In order to measure the coherence in the poloidal direction, the sample volumes are ordered in the poloidal direction on almost the same magnetic surface. For the purpose, the magnetic filed is 1.28 T, and the other parameters are fixed and $q_{95} = 3.2$. The position of the sample volumes are at 1 cm inside the separatrix. The density fluctuation (7 sample volumes), potential and potential fluctuation (4 sample volumes) are measured simultaneously under this condition. The sample volumes are at intervals of 7 mm in the poloidal direction.

The frequency spectra of $\tilde{\phi}$ and normalized \tilde{n}_e are shown in Fig.3(a). Although a peak exists around f_{GAM} in the spectrum of $\tilde{\phi}$, there is no significant peak in the spectrum of normalized \tilde{n}_e . The reason is that the fluctuation with f_{GAM} is weak and the ambient density fluctuation is

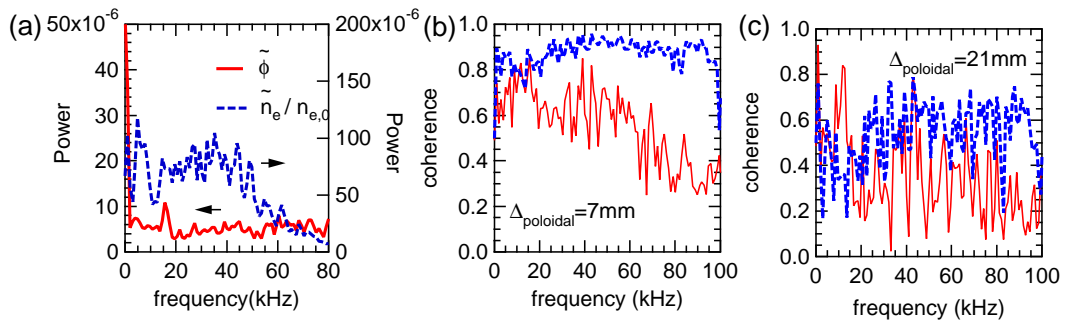


Fig. 3: (a) power spectra of $\tilde{\phi}$ and normalized \tilde{n}_e . (b) Coherence. The sample volumes are at 7 mm apart. (c) Coherence. The sample volumes are at 21 mm apart. The solid line is of $\tilde{\phi}$ and the dashed line is of \tilde{n}_e .

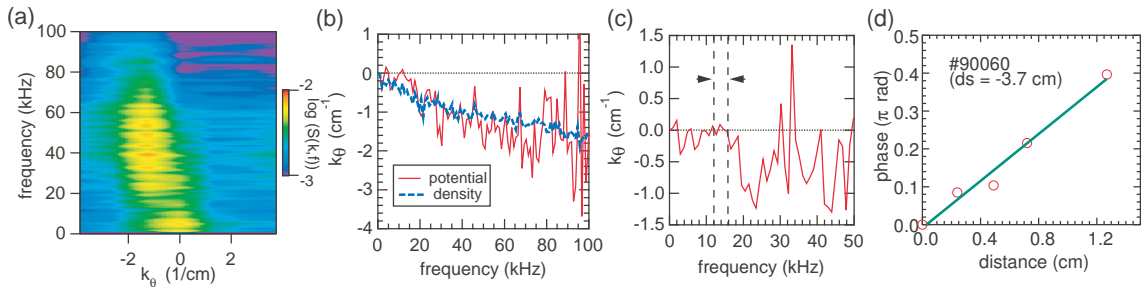


Fig. 4: (a) Dispersion relation of the normalized \tilde{n}_e . (b) Dispersion relation evaluated with phase difference. The sample volumes are at 7 mm apart. (c) Dispersion relation evaluated with phase difference. The sample volumes are at 21 mm apart. The solid line is of $\tilde{\phi}$ and the dashed line is of \tilde{n}_e . (d) phase delay of $\tilde{\phi}(f_{GAM})$ in the radial direction. The horizontal axis is the distance between sample volumes.

strong near the separatrix.

The coherence between the fluctuations is shown in Fig.3(b) and (c). The distance between the sample volumes is 7 mm and 21 mm, respectively. As the distance between the sample volumes is larger, the coherence between \tilde{n}_e signals is smaller in all frequency range. The coherence between $\tilde{\phi}$ signals shows the similar tendency except that $\tilde{\phi}$ near the GAM frequency keeps high coherence. That means the correlation length of $\tilde{\phi}(f_{GAM})$ is longer than that of the ambient fluctuation in the poloidal direction.

4.4 Wave number

First, the poloidal wave number (k_θ) is estimated. The sample volumes can be aligned on almost the same magnetic surface with intervals of 7 mm in the poloidal direction as mentioned above, so we can measure k_θ of 4.5 (cm^{-1}) or less. The dispersion relation of the density fluctuation is estimated with Fast Fourier Transform (FFT) (Fig. 4(a)). The dominant components exist in the frequency range of 40 - 60 kHz and k_θ of 1 - 2 (cm^{-1}). Its poloidal mode number is about 60 - 120.

Because the potential fluctuation is measured only in 4 sample volumes, it is difficult to estimate the dispersion relation with FFT. Thus, the dispersion relation is estimated through the phase difference ($\Delta\varphi$) between the signals from different sample volumes: $k_\theta = \Delta\varphi/\Delta l_p$, where Δl_p is the distance between the sample volumes. The estimated dispersion relation of $\tilde{\phi}$ is shown in Fig. 4(b). The distance of the sample volumes is 7 mm. It is similar to that of \tilde{n}_e . However, k_θ around the GAM frequency is almost zero unlike that of \tilde{n}_e . That is due to $\tilde{\phi}(f_{GAM})$ which has long correlation length in the poloidal direction, so k_θ of $\tilde{\phi}(f_{GAM})$ is estimated using the signals from the sample volumes located at 21 mm apart (Fig.4(c)). The phase difference around the GAM frequency is small, and the k_θ is estimated as $k_\theta = (-2 \pm 24) \times 10^{-3}$ (cm^{-1}). The poloidal mode number is 1.5 or less. It does not contradict the predicted structure of GAM ($m=0$).

Next, in order to estimate the radial wave number (k_r), the sample volumes are set in the radial direction by means of optimization of the magnetic field strength and the energy of the injected heavy ion beam: $B_r = 1.17$ T and $W_0 = 350$ keV. The interval of the sample volumes is about 2.5 mm in the radial direction. The phase difference of $\tilde{\phi}(f_{GAM})$ measured near 3.7 cm inside the separatrix is shown in Fig.4(d)). The k_r is estimated as $k_r = \Delta\varphi_r/\Delta ds$, where $\Delta\varphi_r$ is the phase difference and Δds is the distance between the sample volumes, and $k_r = 0.94 \pm 0.05$ (cm^{-1}). Evaluating k_r through $|E_r| = |-\partial\phi/\partial r| = |k_r\phi|$ in Fig.2, it is consistent with the above k_r . The Larmor radius of the deuteron (ρ_i) is 0.28 cm, where the ion temperature is 380 eV and the magnetic field strength is about 1 T, so $k_r\rho_i = 0.26 < 1$.

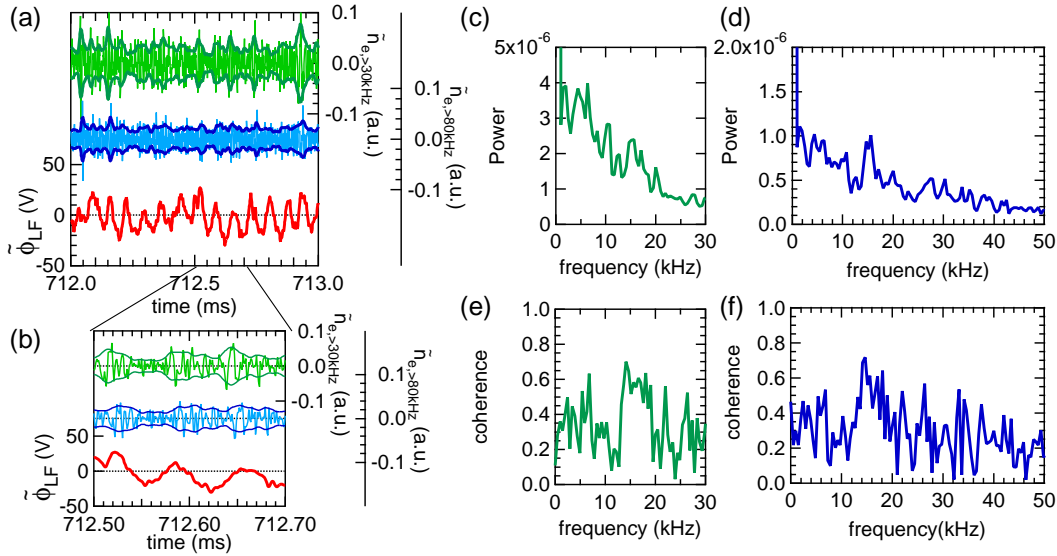


Fig. 5: Relation between \tilde{n}_e and $\tilde{\phi}$. (a): \tilde{n}_e with a frequency of 30 kHz and higher, \tilde{n}_e with a frequency of 80 kHz and higher, and $\tilde{\phi}$ with a frequency from 1 to 30 kHz. The envelope of \tilde{n}_e is also shown. (b): Expanded view of (a). (c) and (d): power spectra of the envelope of \tilde{n}_e in (a). (e) and (f): coherence between $\tilde{\phi}$ and the envelope of \tilde{n}_e .

4.5 The amplitude of $\tilde{\phi}$ and normalized density fluctuation

The relation between the amplitude of $\tilde{\phi}$ and normalized \tilde{n}_e of GAM is predicted as following equation [1]: $|\tilde{n}_e(f_{GAM})/n_{e,0}| = \sqrt{2}k_r\rho_i |e\tilde{\phi}(f_{GAM})/T_e|$. In the experiment, the right hand side of the equation is 11×10^{-3} at -3.7 cm inside the separatrix, where $k_r\rho_i = 0.26$ estimated in the previous section, $|\tilde{\phi}(f_{GAM})|$ is about 11 V (Fig.2(b)), and $T_e = 380$ eV assuming $T_e = T_i$ measured with CXS. The measured $\tilde{n}_e(f_{GAM})/n_{e,0}$ is about 9×10^{-3} , thus the observed fluctuation with f_{GAM} has the same character as that of the predicted GAM.

5 Relation between the fluctuation with the GAM frequency and ambient fluctuation

The fluctuation with f_{GAM} probably produces the shear flow as inferred from Fig.2, so it possibly suppresses the ambient fluctuation. Originally, GAM is produced through nonlinear coupling of the turbulence. Therefore, it can regulate the power of the ambient fluctuation.

In order to see the temporal behavior of the amplitude of the ambient fluctuation, the envelope of \tilde{n}_e is evaluated (Fig.5(a) and (b)). The envelope is evaluated with Hilbert transform and a low pass filter whose cut-off frequency is 30 kHz. The envelope oscillates and it indicates the amplitude of \tilde{n}_e is modulated.

The frequency spectra of the envelopes of \tilde{n}_e with a frequency of 30 kHz or higher ($\tilde{n}_e(f > 30\text{kHz})$) and 80 kHz or higher ($\tilde{n}_e(f > 80\text{kHz})$) are shown in Fig.5 (c) and (d), respectively. A significant peak appears around the GAM frequency in each spectrum. It indicates \tilde{n}_e is modulated with the GAM frequency.

The coherence between the envelope of \tilde{n}_e and $\tilde{\phi}(f_{GAM})$ is shown in Fig.5(e) and (f). There is a peak around the GAM frequency in each figure. Therefore, the modulation of \tilde{n}_e is closely related with the $\tilde{\phi}(GAM)$. It possibly shows the self-regulated mechanism of plasma turbulence with zonal flow (GAM).

Compared with the modulation of $\tilde{n}_e(f > 80\text{kHz})$ with f_{GAM} , that of $\tilde{n}_e(f > 30\text{kHz})$ is weaker

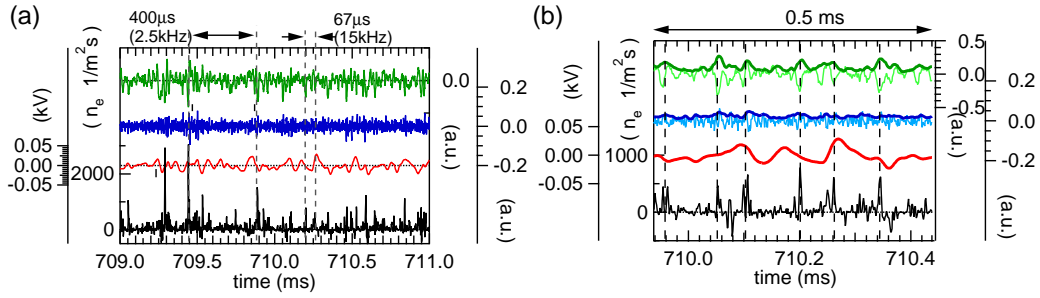


Fig. 6: (a) \tilde{n}_e with a frequency of 30 kHz and higher, \tilde{n}_e with a frequency of 80 kHz and higher, $\tilde{\phi}$ with a frequency from 1 to 30 kHz, and Γ_f in L-mode. (b) the expanded view of (a). The envelope of \tilde{n}_e is also shown.

than the modulation with the lower frequency ($<10\text{kHz}$). It may indicate that the turbulence with higher frequency is suppressed more efficiently by the oscillating shear flow of GAM.

6 Influence on the particle transport

The particle flux induced by the electrostatic fluctuation (Γ_f) can be estimated with \tilde{E}_θ and \tilde{n}_e measured with the HIBP; $\Gamma_f = \tilde{n}_e \tilde{E}_\theta / B_t$. The \tilde{E}_θ is measured by the HIBP through alignment of the sample volumes on the same magnetic surface as described in section 4.3.

In L-mode, the average particle flux $\langle \Gamma_f \rangle$ is about $(80 \pm 40) \times n_e(r_{sv})$ ($1/\text{m}^2 \text{ s}$), where $n_e(r_{sv})$ is the local electron density in the sample volume. Assuming that the particle confinement time is 50 ms which is 5 times the energy confinement time, the particle flux (Γ) is roughly estimated at about 20×10^{19} ($1/\text{m}^2 \text{ s}$). The experimental result is $\langle \Gamma_f \rangle \sim (80 \pm 40) \times 10^{19}$ ($1/\text{m}^2 \text{ s}$), where $n_e(r_{sv}) = 1 \times 10^{19}$ is assumed. Γ_f is the same as Γ in the order, so the measured Γ_f is possibly a major component to the total particle flux.

The measured Γ_f during L-mode is shown in Fig.6. It indicates intermittent behavior. Some spikes appear at intervals of about $67 \mu\text{s}$, which corresponds to f_{GAM} . They coincide with the increase in the amplitude of \tilde{n}_e as shown in Fig.6(b), thus the fluctuation with f_{GAM} affects the particle transport through the modulation of the ambient fluctuation. Larger spikes with longer period (several hundreds μs) also appear in Fig.6(a), and it probably shows the existence of some other mechanism of the intermittent transport.

In this shot, bursting fluctuation appears with the repetition frequency of about 4 kHz just after the start of the formation of the edge transport barrier. After the burst continues for about 9 ms, and \tilde{E}_θ and \tilde{n}_e are suppressed and the transition to the ELM-free H-mode occurs. The burst means the formation and disappearance of a weak transport barrier repeat at intervals of about 4 kHz [15]. $\tilde{\phi}(f_{GAM})$ and any spike with a time interval of GAM period does not appear in the burst phase. Therefore, other mechanism play the important role for the formation of the transport barrier.

7 summary

The characteristic electrostatic potential fluctuation measured by the HIBP is found to have the theoretically predicted characters of GAM: the frequency, the structure in the poloidal direction, wave numbers in radial and poloidal direction, and the relation between amplitude of $\tilde{\phi}(f_{GAM})$ and that of $\tilde{n}_e(f_{GAM})$. Therefore, the fluctuation considered to be GAM.

The high coherence between the envelope of ambient fluctuation and the fluctuation with f_{GAM} clearly indicates that the modulation of the ambient fluctuation and the fluctuation with f_{GAM} is closely related.

The measured particle flux indicates the intermittent behavior. The fluctuation with f_{GAM} affects the particle transport through the modulation of the ambient fluctuation, however, it seems that the intermittent flux can not be explained only with the effect of GAM. And, it does not appear in H-mode and bursting phase but in L-mode and Ohmic phase. Therefore, other mechanism play the important role for the formation of the transport barrier.

Acknowledgement

We are grateful to Professor K. Itoh, Professor K. Toi, Dr. A. Fujisawa, Dr. Y. Kishimoto, Dr. T. Matsumoto, and Dr. N. Miyato for fruitful discussions, and Dr. H. Ninomiya, Dr. M. Kikuchi, Dr. H. Kimura, Dr. M. Azumi, Dr. H. Kishimoto, Professor M. Fujiwara, and Professor O. Motojima for the continuous encouragement. We would like to thank Dr. Y. Uesugi for valuable suggestions. This work was carried out as a joint work under the Facility Utilization Program of JAERI.

References

- [1] For review, see P. H. Diamond, S.-I. Itoh, K. Itoh, and T.S. Hahm, Plasma Phys. Control. Fusion in press
- [2] Z. Lin, T. S. Hahm, W. W. Lee, W. M. Tang, and R. B. White, Science **281** (1998) 1835
- [3] P. H. Diamond and et al., in Proceedings of the 17th IAEA fusion energy conference, Yokohama, 1998 **4** 1421. (International Atomic Energy Agency, Vienna, Austria, 1999)
- [4] M. G. Shats and W. M. Solomon, Phys. Rev. Lett. **88** (2002) 045001
- [5] G.R. McKee, and et al., Phys. Plasma, **10** (2003) 1712
- [6] G.S. Xu, B.N. Wan, and J. Song, M. Li, Phys. Rev. Lett. **91** (2003) 125001
- [7] A. Fujisawa and et al., Phys. Rev. Lett. in press
- [8] Y. Hamada and et al., submitted to Nucl. Fusion
- [9] N. Winsor, J. L. Johnson, and J. M. Dawson, Phys. Fluids **11** (1968) 2448
- [10] K. Hallatschek and D. Biskamp, Phys. Rev. Lett. **86** (2001) 1223
- [11] A. Fujisawa, H. Iguchi, S. Lee, and Y. Hamada, Rev. Sci. Instrum. **68** (1997) 3393
- [12] T. Ido, and et al., Rev. Sci. Instrum. **70 partII** (1999) 955
- [13] T. Ido, and et al., Plasma Phys. Control. Fusion **41** (1999) 1013
- [14] T. Ido, and et al., Phys. Rev. Lett., **88** (2002) 055006
- [15] Y. Miura, and et al., Nucl. Fusion, **41** (2001) 973